

URTeC: 2669946

## Geomechanics of the Microseismic Response in Devonian Organic Shales at the Marcellus Shale Energy and Environment Laboratory (MSEEL) Site, West Virginia

Erich Zorn<sup>1\*</sup>, William Harbert<sup>1,2</sup>, Richard Hammack<sup>1</sup>, Abhash Kumar<sup>1,3</sup>

<sup>1</sup> National Energy Technology Laboratory, US Department of Energy, Pittsburgh, PA

<sup>2</sup> Department of Geology and Environmental Science, University of Pittsburgh, PA

<sup>3</sup> AECOM

Copyright 2017, Unconventional Resources Technology Conference (URTeC) DOI 10.15530/urtec-2017-2669946

This paper was prepared for presentation at the Unconventional Resources Technology Conference held in Austin, Texas, USA, 24-26 July 2017.

The URTeC Technical Program Committee accepted this presentation on the basis of information contained in an abstract submitted by the author(s). The contents of this paper have not been reviewed by URTeC and URTeC does not warrant the accuracy, reliability, or timeliness of any information herein. All information is the responsibility of, and, is subject to corrections by the author(s). Any person or entity that relies on any information obtained from this paper does so at their own risk. The information herein does not necessarily reflect any position of URTeC. Any reproduction, distribution, or storage of any part of this paper without the written consent of URTeC is prohibited.

---

### Abstract

Using an innovative workflow incorporating microseismic attributes and geomechanical well logs, we have defined major geomechanical drivers of microseismic expression to understand reservoir stimulation response in engineering and geological contexts. We sampled microseismic data from two hydraulically fractured Marcellus wells in the Appalachian Basin, northern West Virginia, vertically through the event cloud, crossing shale, limestone, sandstone, and chert. We focused our analysis on the Devonian organic shale and created pseudo-logs of moment magnitude ( $M_w$ ), b-value, and event count. The vertical moving-average sampling of microseismic data was completed such that the sample interval matched that of the geophysical well log. This technique creates robust, high-resolution microseismic logs that show subtle changes in microseismic properties and allows direct cross-plotting of microseismic versus geophysical logs. We chose five geomechanical properties to form the framework against which to interrogate the microseismic data: Young's modulus (YM), Poisson's ratio (PR), brittleness, lambda-rho ( $\lambda\rho$ ), and mu-rho ( $\mu\rho$ ). Additionally, we included natural gamma as a useful measure of organic content. Having defined this microseismic-geomechanical cross-plot space, we derived insights into the response of these units during hydraulic fracturing. Observations include: 1) larger magnitude microseismicity occurs in high PR, high YM rocks; high event counts are found in low PR rocks; 2) low b-value (high in-situ stress) is consistent with the occurrence of larger magnitude events and low event counts; and 3) YM and PR act as bounding conditions, creating "sweet spots" for high and low  $M_w$ , event count, and stress. In our cross-plot space, there is a meaningful link between microseismicity and the elastic properties of the host rock. In light of this dependence of stimulation potential on elastic properties, the calculation of microseismic pseudo-logs at stimulation sites and application of our cross-plot framework for microseismic-geomechanical analysis in unconventional shale will inform operators in planning and forecasting stimulation and production, respectively.

### Introduction

In late 2015, two parallel, horizontal wells in Monongalia County, West Virginia were drilled and hydraulically fractured in the Marcellus Shale over 58 stages (Figure 1). The wells were stimulated separately from each other, with the more northerly well (Well 5) completed first, then the southerly well (Well 3) second, as opposed to a "zipper-frac" or simulfrac. Microseismic monitoring was completed by Schlumberger, deploying one 12-level (100 foot spacing) Versatile Seismic Imager (VSI<sup>TM</sup>) array down one vertical deep well. Additionally, standard well logs including p-sonic, s-sonic, bulk density, total porosity, and natural gamma were acquired in the vertical well, and a full suite of geomechanical well logs were acquired along the length of one of the horizontal wells.

25,116 microseismic events were recorded at the geophones over the course of 52 out of the 58 stages of treatment (Figure 1), ranging between moment magnitude ( $M_w$ ) -3.15 and -0.05, with a mean value of  $M_w$  -2.14. The seismicogenic  $b$ -value is simply the slope of the linear portion of the  $\log_{10}$  (frequency) versus magnitude distribution in a seismic catalog, and is an indicator of in-situ stress conditions. We employed the seismological toolset ZMAP (Wiemer 2001). The completeness magnitude ( $M_c$ ) is the minimum magnitude above which the distribution still follows the Gutenberg-Richter power law relationship.  $M_c$  for this dataset varies between -1.8 and -2.2 depending upon the method of calculation.  $M_c$  can be calculated by modelling the catalog for the entire magnitude range and determining the point at which the distribution becomes non-linear or non-self-similar. This is known as the EMR method (Woessner 2005). A simpler method is to find the point of maximum curvature (MaxC) in the frequency-magnitude distribution. The overall  $b$ -value for the entire catalog from both wells ranges between 1.2 and 1.5, depending upon the  $M_c$  calculated.

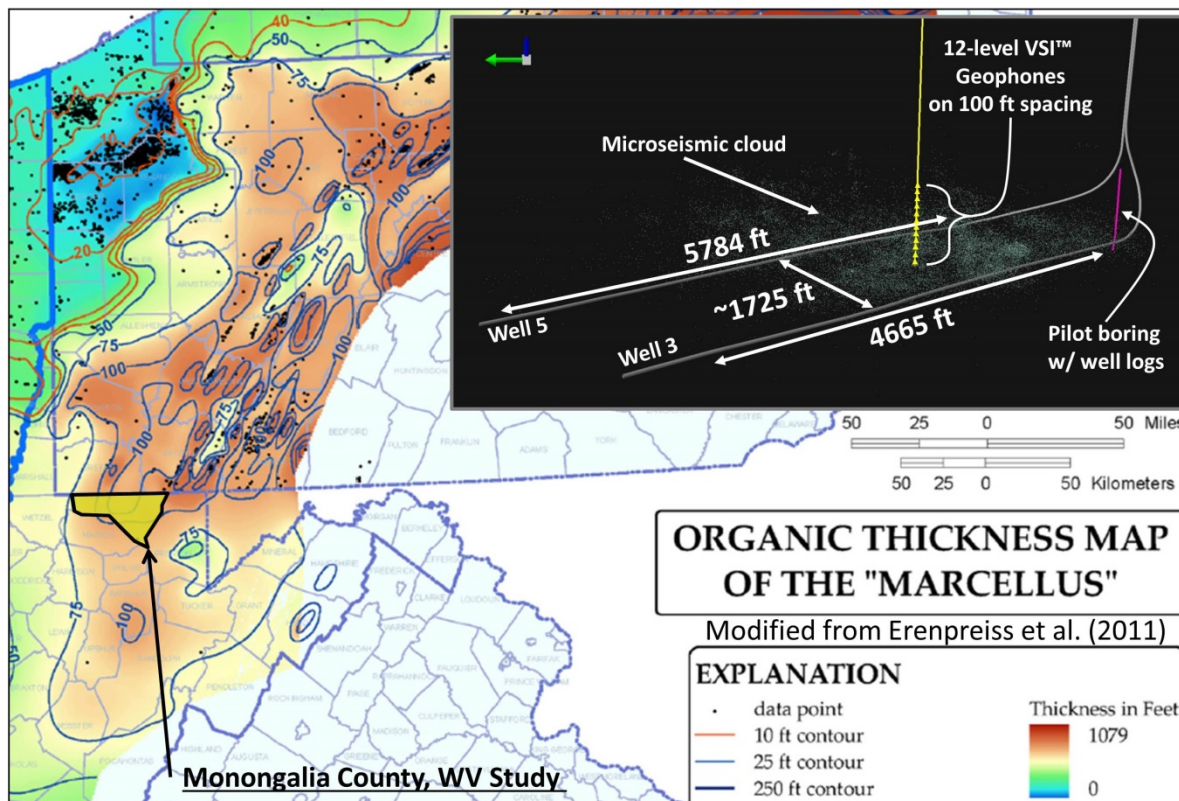


Figure 1. Location map, modified from Erenpreiss et al. (2011). Inset is a view of the lateral well geometry and spacing, monitoring well location and configuration, logged pilot hole location and depth, and the microseismic cloud.

In the development of unconventional resources like the Marcellus Shale, where natural gas is trapped within tight and/or poorly interconnected porosity, direct stimulation of the source/reservoir layer through hydraulic fracturing is critical to the recovery of hydrocarbons. Microseismic monitoring provides direct evidence of fracture formation by detecting the resulting seismic events, as documented in Maxwell et al. (2002) and other studies. However, not all of the hydraulic energy transferred downhole is applied to the task of creating fractures in the zone of interest. Much of this energy is lost to heat, fluid energy dissipation, and aseismic deformation (Lee et al. 1991, Boroumand and Eaton 2012). Furthermore, the majority of microseismicity occurs outside of the zone of interest. The inefficiency described above should be accounted for when using microseismic data as a measure of stimulation. A too simplistic approach in which abundant microseismicity should correspond to high hydrocarbon production can lead to over- or under-estimates of production. However, the distribution of microseismicity over a vertical span that includes four distinct shale units and multiple limestone units presents the opportunity to examine the relationship between rock mechanical properties and microseismic characteristics. Roche and van der Baan (2015) performed similar work in which they investigated the effect of in-situ stress, pore pressure, lithological layering and coupling, and geomechanical rock properties on the distribution and characteristics of microseismicity at two hydraulic fracturing sites.

**Methods**

In order to directly compare properties of the microseismic catalog such as event magnitude and event count to the geophysical well logs, the microseismic cloud was sampled using a five-foot vertical window that was advanced through the cloud at the same interval and elevation as the well logs (Figure 2a). First, using ZMAP (Wiemer 2001), the b-value was calculated for the entire microseismic catalog, and the corresponding completeness magnitude ( $M_c$ ) was used as a cutoff (Figure 2a; Figure 3), eliminating events with magnitudes too small to be detectable uniformly across the entire site, as described in Maxwell (2012).  $M_c$  is represented on Figure 2a by the sharp cutoff in the microseismic cloud. The moment magnitude of events within the window at each sampling point was averaged to create a moment magnitude “log”. The number of events within the moving window at each sampling point was also used to create an event count log. Lastly, using the complete dataset, the slope of the frequency-magnitude distribution (b-value) of microseismicity within a dynamically sized, sliding sample window containing 300 events, was calculated to create a b-value log. This robust b-value log was then interpolated to match the well log sample interval. Figure 2b shows the core set of geomechanical and microseismic logs used in this study.

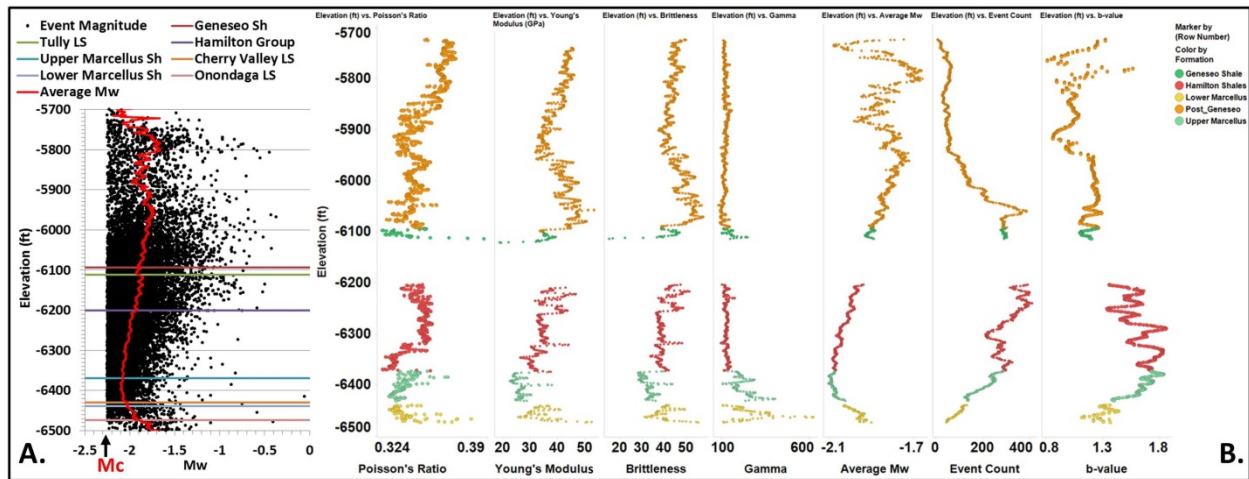


Figure 2. (A) The moment magnitude “log” superimposed on the microseismic cloud from which it was calculated. (B) The geomechanical / dynamic moduli logs and microseismic logs forming the foundation of the analyses in this study.

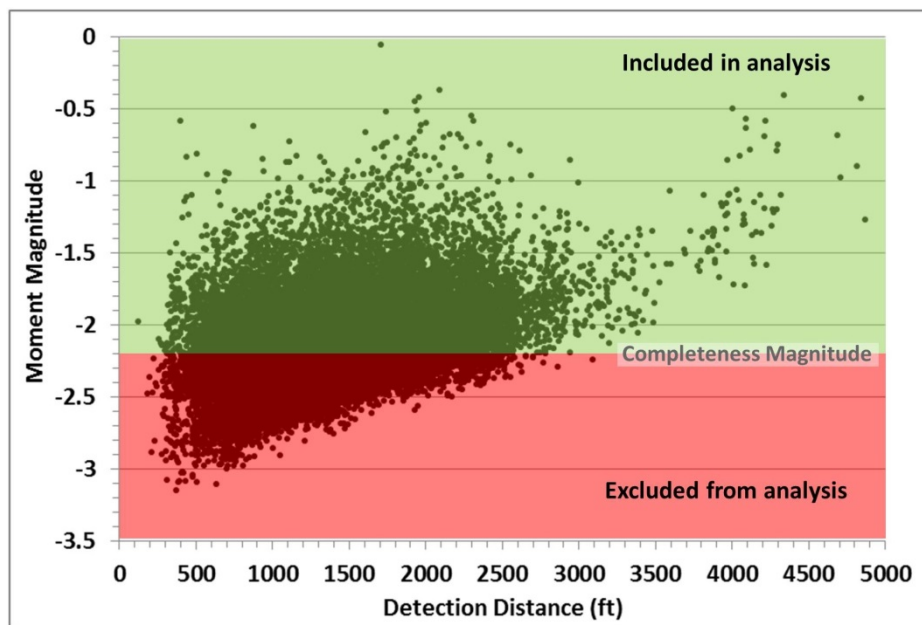


Figure 3. Moment magnitude versus detection distance (ft), showing the naturally inclined detection threshold, indicating a decrease in small magnitude detection ability with increased distance. The plot is divided into two panels, based upon a completeness magnitude of -2.2.

The mu-rho versus lambda-rho (MRLR) crossplot forms the foundation upon which these other properties are imposed because they are invariant and form the basic elements of the other moduli. Goodway et al. (2010) illustrated the usefulness of the MRLR space in describing changes in lithology, porosity, elasticity, and fluid content (among other properties) (Figure 4). Our approach in this study is to crossplot MRLR and color the data cloud by one of the microseismic parameters, while superimposing useful reference iso-lines of PR, YM, and brittleness, and shading the plot by gamma value. We consider this crossplot space the most useful in interpreting our attributes. This approach of displaying seven attributes in a single reference plot helps to identify the principal components that drive change in microseismic expression. Brittleness is calculated according to Rickman et al. (2008), in which PR and YM alone describe brittleness:

$$BRIT\_YM = ((YM - 1)/(8 - 1)) * 100$$

$$BRIT\_PR = ((PR - 0.4)/(0.15 - 0.4)) * 100$$

$$BRIT\_TOTAL = ((BRIT\_YM + BRIT\_PR) / 2)$$

In these equations, it is important to note the YM and PR threshold values that affect the total brittleness calculation. When YM = 8 Mpsi and PR = 0.15, the resulting material will be “100%” brittle. YM = 1 Mpsi and PR = 0.4 will produce a “0%” brittle material. Reasonable combinations of values are likely constrained within these bounds, resulting in brittleness values of between 0 and 100%. As YM increases, brittleness increases; as PR increases, brittleness decreases.

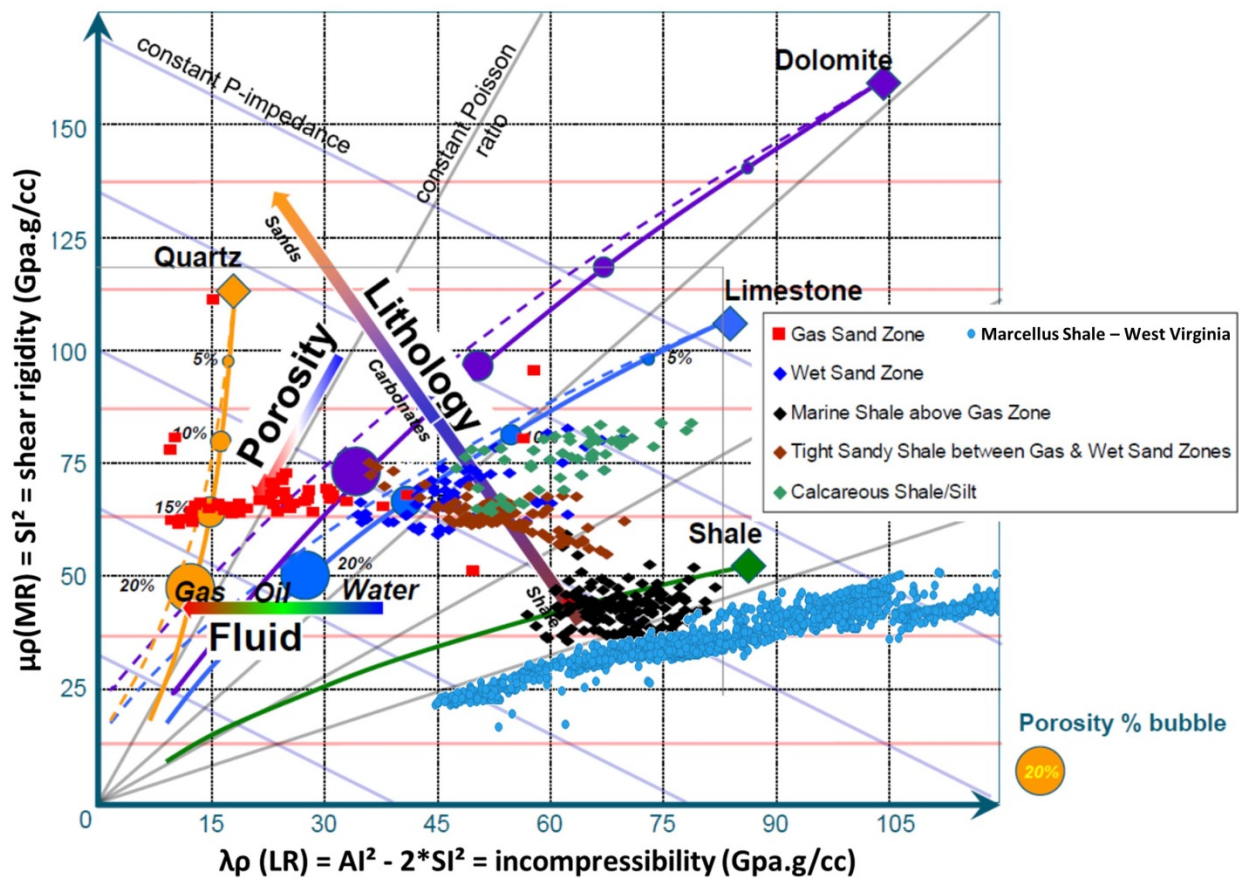


Figure 4. The utility of Mu-Rho versus Lambda-Rho space, with West Virginia Devonian Shale data superimposed in light blue. Modified from Goodway (2009).

To reduce detection bias in the microseismic data, we excluded all events with a moment magnitude smaller than the magnitude of completeness (-2.2) of the microseismic catalog, as defined by the b-value of the frequency-magnitude

distribution (Figure 2a, identified by Mc; Figure 3). Location uncertainty ranges from an average of 160 feet in the maximum eigenvector dimension to 42 feet in the minimum dimension. To minimize error we excluded all microseismic events with a signal to noise ratio  $< 2$ . Stratigraphically, at the project scale, rock units are relatively flat lying and laterally continuous. This is important due to the nature of the sampling and analysis methods being employed here, in which well log properties are treated as laterally applicable and uniform. As this present study concentrates only on the geomechanical and microseismic properties of organic shale, we excluded any non-shale rocks from the analysis, such as limestone and chert. In an effort to be consistent with a previous study completed in Clearfield County, PA (Zorn et al. 2017), we decided to use the same basic log set of  $V_p$ ,  $V_s$ , and  $Rho_B$  (bulk density) as the starting point for all calculations. It is understood that there is uncertainty in both the location and magnitude of microseismic events, and also in the assumption that rock layers are flat lying and laterally continuous. We feel that the sampling methods employed in this study (sliding/overlapping sampling windows, average magnitudes, etc.) are robust enough to soften the effects of this uncertainty.

## Results

In order to approach the interpretation of this projection of seven different variables, we first examine the data for gradients present at orthogonal angles to iso-lines of each variable. In examining the data-cloud against YM, we see direct correlation between increasing or decreasing YM and the presence of relatively large or small moment magnitude events, respectively (Figure 5). Additionally, when we examine the data compared to iso-lines of PR, a relationship emerges in which the smallest magnitude microseismicity generally occurs in the zone of lowest PR and the largest magnitude microseismicity occurs in the zone of highest PR.

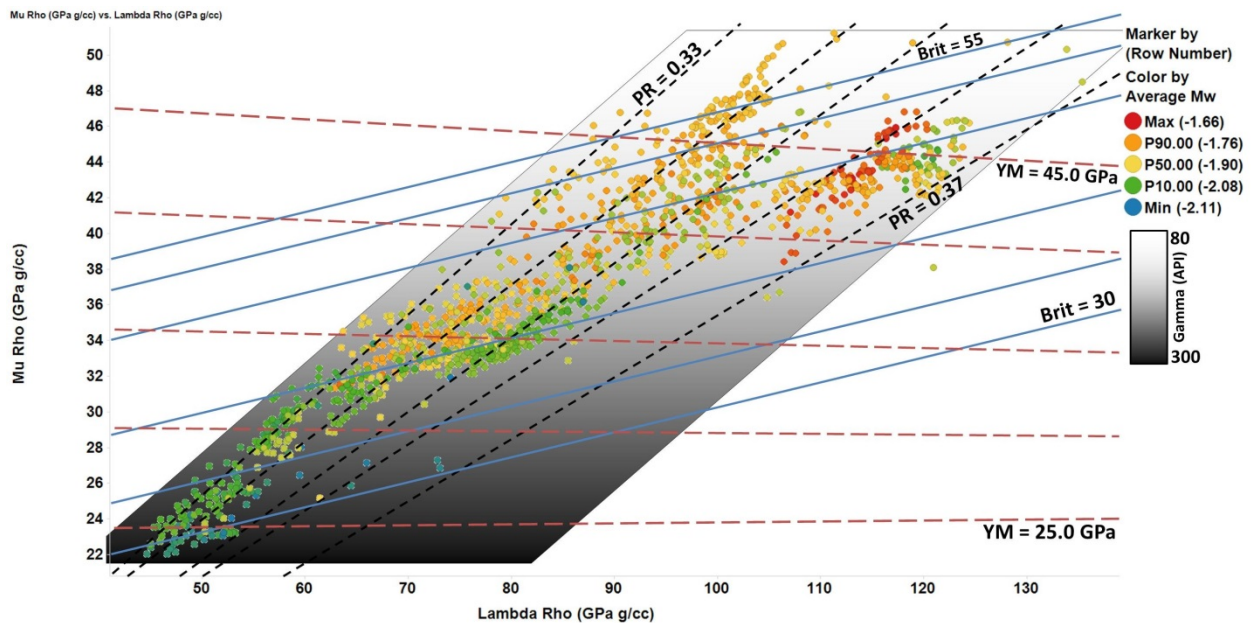


Figure 5. The MRLR analysis space colored by average moment magnitude of microseismicity.

It appears that PR exerts first order control over the relative abundance of microseismicity (Figure 6). There is a striking juxtaposition of the highest event count next to lowest event count, within the same zone of YM ( $> 40$  GPa). However, the lowest number of events occurs at the highest PR, and microseismicity is most abundant where PR is lowest. Examination of the zone of low PR reveals there is a secondary gradient in which a combination of high YM and low PR conditions will result in more microseismicity than a low YM / low PR condition.

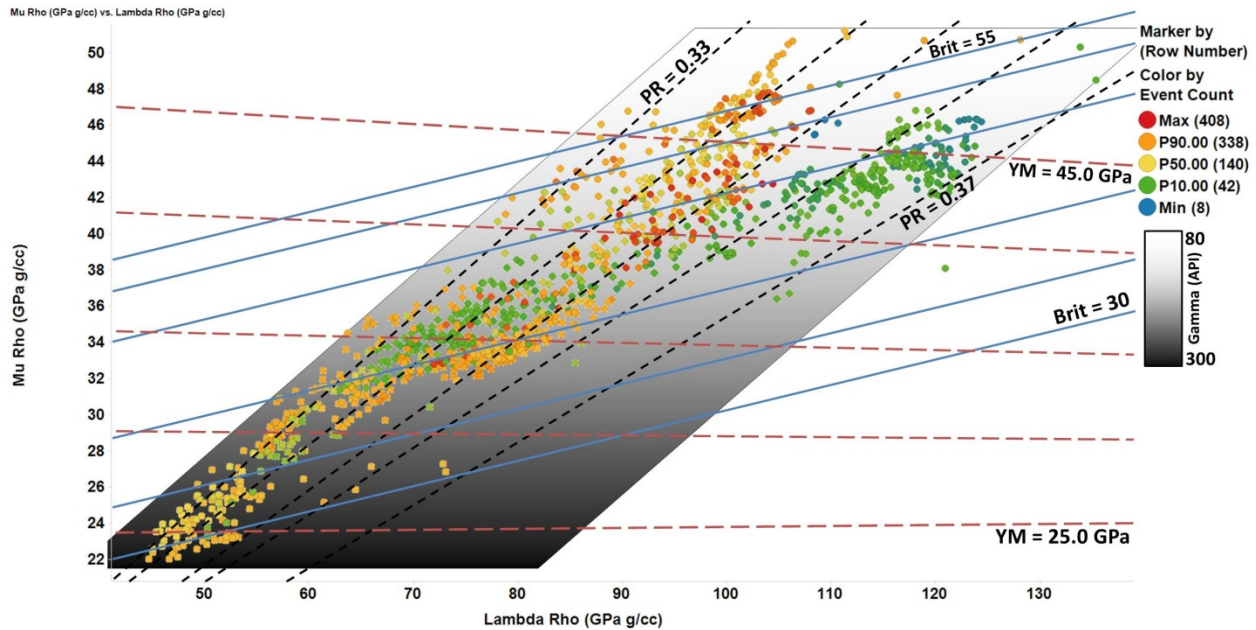


Figure 6. The MRLR analysis space colored by microseismic event count.

The seismogenic  $b$ -value can be interpreted as an indicator of stress condition (Schorlemmer et al. 2005, Goertz-Allmann and Wiemer 2013). A low  $b$ -value indicates that a larger proportion of the event catalog is comprised of larger magnitude seismicity, conceivably a result of higher stress conditions at failure. Conversely, a high  $b$ -value ( $>1$ ) indicates a distribution of seismicity weighted more toward smaller magnitudes as a result of failure in a lower stress condition. In MRLR space, according to Goodway, the state of in-situ stress increases with increasing MR and LR. We observe the lowest  $b$ -values in the region of the crossplot that generally corresponds to the largest moment magnitudes and lowest event counts (Figure 7). Relating to rock physical properties, low  $b$ -values occur in mid to high YM and lower gamma (organic content) rocks. Conversely, the highest  $b$ -values occur in rocks with a low YM and the highest organic content. A low YM and high organic content would presumably allow internal stresses to be redistributed more readily, discouraging a high stress condition and resulting in a higher  $b$ -value.

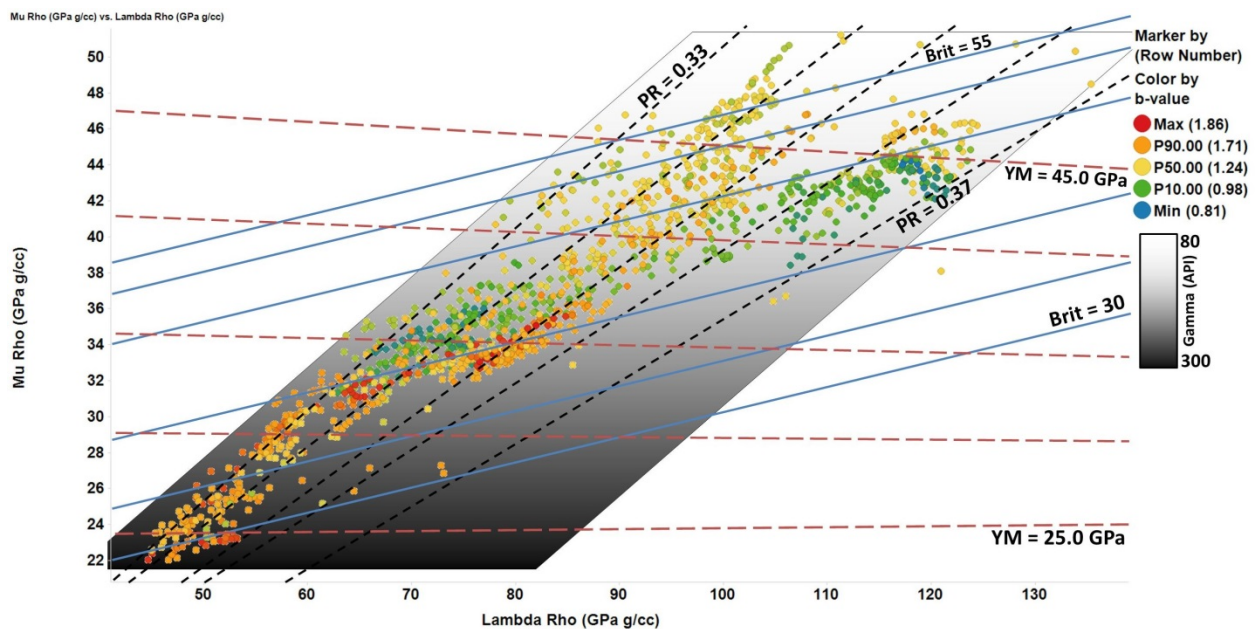


Figure 7. The MRLR analysis space colored by the seismogenic  $b$ -value of microseismicity.

## Discussion

Young's modulus (axial stress / axial strain) is a measure of material stiffness and Poisson's ratio (axial strain / lateral strain) is a measure of material toughness (Figure 8). Stiffness is the resistance to deformation when stressed, while toughness is the resistance to fracturing when stressed. Stiff materials are generally more brittle and prone to fracturing, and resistant to deformation, while less stiff materials are tougher. A material that possesses a high PR will likely have a low YM, and vice versa, but there is a natural spread in the possible physical value combinations such that at a given stiffness, materials can be more or less tough, and at a given toughness, materials can be more or less stiff. We believe that the observed relationships between microseismic properties and elastic properties of organic shale rocks are a result of these subtle interactions between YM and PR. Of course, there are second-order variables which undoubtedly influence these relationships, such as existing structures (expulsion features, fractures, faults, or other stress risers), in-situ pore pressure, pore shape, permeability/diffusivity, clay and kerogen content, differential stress/closure stress, anisotropy, pumping pressure, rate, volume, and duration. We have tried to address the matter of stress state through the inclusion of b-value analysis. The effect of relative organic content and its relationship with geomechanical and microseismic properties can be seen in the gamma value overlay.

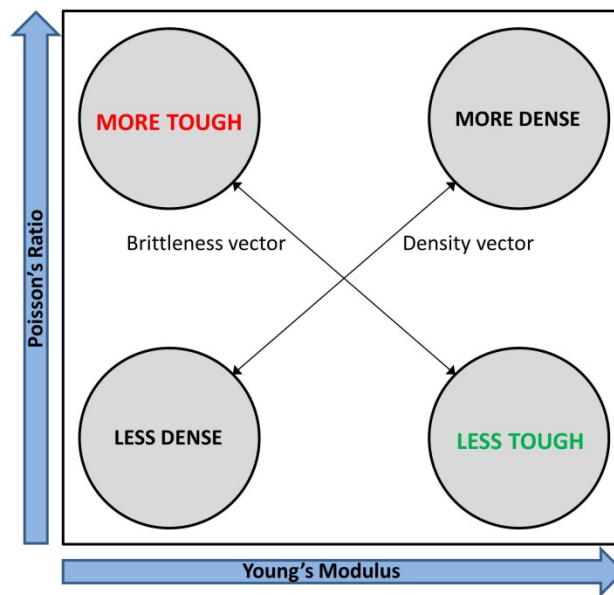


Figure 8. Poisson's Ratio versus Young's Modulus crossplot space and the distribution of elastic rock properties.

We observe in Figure 5 that the reservoir rocks with the highest PR and YM also host the largest average magnitude microseismicity. These are both the toughest and stiffest rocks, meaning they are both resistant to fracturing and resistant to deforming. The inverse is also apparent: the smallest magnitude microseismicity occurs in formation rocks with the lowest YM and the lowest PR.

In the examination of microseismic event count in the context of geomechanical properties (Figure 6), we see a first order gradient in which rocks with the lowest PR host the largest number of microseismic events. A second order gradient orthogonal to YM indicates that at any value of PR, an increasing YM will cause an increase in the occurrence of microseismicity. No data resides in the low YM, high PR zone of the crossplot, as this combination of rock mechanical properties does not exist in this stratigraphic sequence. However, one can extrapolate that in a rock that is highly resistant to fracturing and amenable to deformation, the formation of brittle fractures and associated microseismicity would be a rare occurrence. The zone of maximum event count on the MRLR plot spans the spectrum of YM values but is focused on the low PR area, where rocks are more prone to fracturing. It should be noted that in comparing the distribution of moment magnitude and event count in Figure 5 and Figure 6, we observe that the small to mid-size magnitudes coincide with a greater abundance of microseismicity and the largest magnitudes coincide with the lowest event counts. This is important as it demonstrates, in an induced microseismic catalog, adherence to frequency-magnitude laws set forth by Gutenberg and Richter (1944).

The analysis and discussion of b-value is relevant because it directly relates the magnitude to the abundance of microseismicity and we have shown that these three seismological attributes are in agreement, i.e. large  $M_w \rightarrow$  low event count  $\rightarrow$  low b-value, and small  $M_w \rightarrow$  high event count  $\rightarrow$  high b-value. More importantly, however, is the interpretation of b-value as an indicator of the in-situ stress state at the point of failure. Locally, the state of stress is influenced by the ability of the rock to distribute that stress, which is a function of the shale lithology and microstructure in the area of failure. Figure 7 illustrates that the highest b-values correspond to the lowest values of YM and PR, indicating that an increased ability to deform and/or sustain a fracture in response to stress discourages the development of a high local state of stress. The opposite relationship is also observed, in which the region of highest YM and PR corresponds to the presence of the lowest b-values. Additionally, it appears that there is a relationship between b-value and gamma value. If gamma is treated as a gross estimator of relative organic or kerogen content, then the most organic-rich shale will be least resistant to deformation in response to stress, and therefore have a tendency to host high b-value microseismicity.

## Conclusions

We have approached a greater understanding of the fundamental geomechanical influences on the microseismic response to hydraulic fracturing. Utilizing standard sonic and density well logs, we calculated the dynamic elastic moduli, and employed a novel approach to create comparable microseismic “logs”. A multi-dimensional MRLR crossplot facilitated a dense and efficient display of meaningful data and uncovered subtle relationships between elastic properties of organic shale and the seismological attributes of recorded microseismicity. PR exerts a strong influence on the average moment magnitude of seismicity. PR and YM influence the abundance and frequency-magnitude distribution of seismicity. The elasticity of the rock, in the context of toughness and stiffness, directly affects the local in-situ state of stress, which in turn, affects the magnitude and abundance of microseismicity.

In terms of importance to energy industry applications, this knowledge can help to refine the concepts of “fracability” and “stimulated” reservoir. Traditionally, more microseismicity translates to “more fracable”. Targeting low PR rocks will result in increased event counts. Additionally, low PR is thought to correlate with higher exploitable organic content and a larger number of existing micro-fractures and/or expulsion features. However, these events will generally be the smallest magnitudes. Moment magnitude ( $M_w$ ) is related to the area of the rupture plane and the stress drop at the failure, and the energy release of the failure increases logarithmically on the  $M_w$  scale. There may be some validity to targeting organic shale at the highest end of the PR scale and mid-high YM. Although event count will decrease, energy release and area of the failure plane will increase. High PR translates to larger average moment magnitude, and mid-high YM translates to a greater ability to sustain a propped fracture.

Finally, there are myriad other factors that can be less accessible but need to be kept in mind. These may act as additional controls on the microseismic response, including: existing macro and micro-structure (expulsion features, fractures, faults, or other stress-risers), in-situ pore pressure, pore shape, permeability/diffusivity, clay and kerogen content, differential stress/closure stress, anisotropy, pumping pressure/rate/volume/duration. We have established a foundation of understanding from fundamental material properties upon which to build in additional complexity.

## Acknowledgements

We would like to thank the US Department of Energy’s National Energy Technology Laboratory and their industry partners for making this work possible.

## References

- Boroumand, N., and D. W. Eaton, 2012, Comparing energy calculations: Hydraulic fracturing and microseismic monitoring: GeoConvention 2012: Vision, 1-4.
- Erenpreiss, M. S., L. H. Wickstrom, C. J. Perry, R. A. Riley, and D. R. Martin, 2011, Regional organic thickness map of the Marcellus Shale. Ohio Department of Natural Resources, Division of Geological Survey, 6 April 2011, [https://geosurvey.ohiodnr.gov/portals/geosurvey/Energy/Marcellus/Regional\\_Marcellus%20thickness\\_cntrlpts\\_8x11.pdf](https://geosurvey.ohiodnr.gov/portals/geosurvey/Energy/Marcellus/Regional_Marcellus%20thickness_cntrlpts_8x11.pdf) (accessed 12 June 2017).
- Goertz-Allmann, B. P., and S. Wiemer, 2013, Geomechanical modeling of induced seismicity source parameters and implications for seismic hazard assessment: *Geophysics*, 78, no. 1, KS25-KS39.
- Goodway, W., M. Perez, J. Varsek, and C. Abaco, 2010, Seismic petrophysics and isotropic-anisotropic AVO methods for unconventional gas exploration: *The Leading Edge*, 29, no. 12, 1500-1508.
- Gutenberg, B., and C. F. Richter, 1944, Frequency of Earthquakes in California: *Bulletin of the Seismological Society of America*, 34, no. 4, 185-188.
- Lee, T. S., S. H. Advani, and J. M. Avasthi, 1991, Characteristic-time concept in hydraulic fracture configuration evolution and optimization: *SPE Production Engineering*, 6, no. 3, 323-333.
- Maxwell, S., 2012, Comparative microseismic interpretation of hydraulic fractures, Paper SPE-162782: SPE Canadian Unconventional Resources Conference, Proceedings, 1-8.
- Maxwell, S. C., T. I. Urbancic, N. Steinsberger, and R. Zinno, 2002, Microseismic imaging of hydraulic fracture complexity in the Barnett Shale, Paper SPE-77440: SPE Annual Technical Conference and Exhibition, Proceedings, 1-9.
- Rickman, R., M. Mullen, E. Petre, B. Grieser, and D. Kundert, 2008, A practical use of shale petrophysics for stimulation design optimization: all shale plays are not clones of the Barnett Shale, Paper SPE-115258: SPE Annual Technical Conference and Exhibition, Proceedings, 1-11.
- Roche, V., and M. van der Baan, 2015, The role of lithological layering and pore pressure on fluid-induced microseismicity: *J. Geophys. Res. Solid Earth*, 120, no. 2, 923-943.
- Schorlemmer, D., S. Wiemer, and M. Wyss, 2005, Variations in earthquake-size distribution across different stress regimes: *Nature*, 437, 539-542.
- Wiemer, S., 2001, A software package to analyze seismicity: ZMAP: *Seismological Research Letters*, 72, no. 2, 374-383.
- Woessner, J. (2005). "Assessing the Quality of Earthquake Catalogues: Estimating the Magnitude of Completeness and Its Uncertainty." *Bulletin of the Seismological Society of America*, 95, no. 2. 684-698.
- Zorn, E.V., W. Harbert, R. Hammack, A. Kumar, 2017, Geomechanical lithology-based analysis of microseismicity in organic shale sequences: a Pennsylvania Marcellus Shale example: *The Leading Edge*, In Press.